Electronic Supplementary Material (ESI) for RSC Advances.

High catalytic performance of Al-Pd-(Ru, Fe) icosahedral approximants for acetylene semi-hydrogenation.

*Keishi Abe[1, 2], Ryota Tsukuda[1, 2], Nobuhisa Fujita[2], *Satoshi Kameoka[2]*

[1] Department of Materials Processing, Graduate School of Engineering, Tohoku University, Aoba-yama 6-6-02, Aoba-ku, Sendai, 980-8579, Japan

[2] Institute of Multidisciplinary Research for Advanced Materials, Tohoku University, Katahira 2-1-1, Aoba-ku, Sendai, 980-8577, Japan

1. The manufacturing process of each alloy.

Pieces of Al, Pd, Ru, and Fe were mixed in an arc-melting furnace under an Ar atmosphere, and as-cast alloys typically got about 5 g. Their purity of Al was 99.9%, of Pd 99.99%, of Ru 99.95%, and of Fe 99.9%. Each sample was annealed at a temperature for a time specified in **Table S1**. The primitive cubic approximant, P_{40}-AlPdRu, with a space group $Pa\bar{3}$ and lattice constant about 40 Å, exists on the Ru-rich end of the Al-Pd-Ru icosahedral quasicrystal[S1, S2]. Its Ru-low region exists P_{20}-AlPdRu with a lattice constant of about 20 Å that is also cubic approximant[S1]. The primitive cubic approximant, *C*-AlPdFe, with space group $Pm\bar{3}$ and lattice

constant of about 7.7 Å, exists in the same chemical composition rate of P_{40}-AlPdRu[S3, S4]. More detailed phase information for each chemical composition prepared for this work was shown in **Table S1**. And the detail structure of the approximant was described in "Crystal structure of the Al-Pd-TM icosahedral approximants" section.

$Al_{13}Fe_4$, Al_3Pd_2 and Al_2Ru were used as comparison of catalytic property. The monoclinic structure of $Al_{13}Fe_4$ **Figure S1(a)** belongs to the $C2/m$ space group with following lattice parameters: a = 15.492 Å, b = 8.078 Å, and c = 12.471 Å, with β = 107.69°[S5]. The polygons represent Henley-type clusters of $Al_{13}Fe_4$, which are composed of a ten-fold flat plane of Al and Fe and stacked pentagonal pyramids of Al_5Pd. It was annealed at 1060 ˚C with a composition of Al-11.5 at.% Fe. The trigonal structure of Al_3Pd_2 belongs to the space group $P\bar{3}m1$. It is a simpler IMC that is composed of 12 atoms per unit cell (**Figure S1(b)**) with the following lattice parameters: a = 4.219 Å, c = 5.160 Å[S6]. It was annealed at 900 ˚C with the composition of Al-40 at.% Pd. The orthorhombic structure of Al_2Ru belongs to the space group *Fddd*. It is also a simpler IMC that is composed of 24 atoms per unit cell (**Figure S1(c)**) with the following lattice parameters: a = 4.710 Å, b = 7.990 Å, c = 8.760 Å[S7]. It was annealed at 1000 ˚C with the composition of Al-33.3 at.% Ru. The annealed time for each sample was 120 h. Al_3Pd_2 and Al_2Ru don't have complex structure such as $Al_{13}Fe_4$ and approximants. The powder XRD pattern obtained from the $Al_{13}Fe_4$, Al_3Pd_2 and Al_2Ru IMCs were shown in **Figure S2**. It was not observed impurity peaks in the respective IMCs.

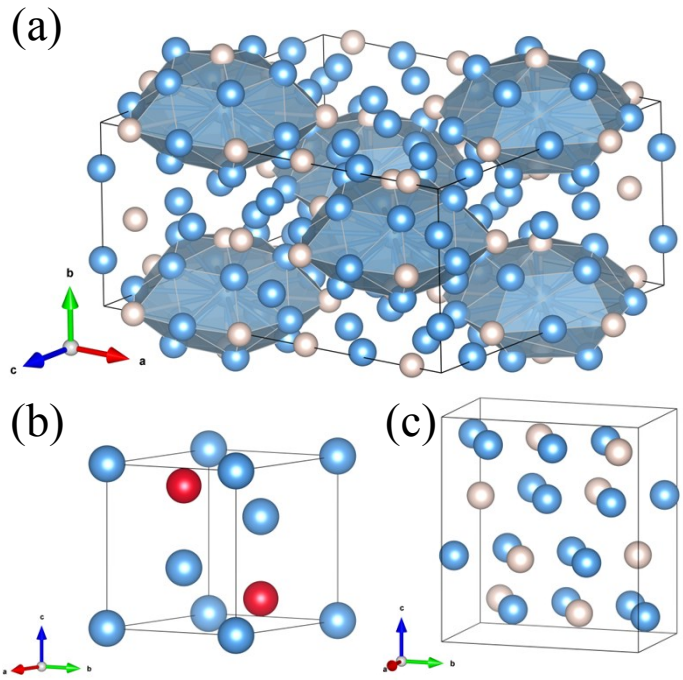

Figure S1. Crystal structure of ICMs. (a) $Al_{13}Fe_4$, (b) Al_3Pd_2 and (c) Al_2Ru: Al, blue; Pd, dark read; Fe, Ru; light pink.

Table S1. Crystallographic data and annealing condition.

Specimen	S.G. or symmentry	Lattice constant (quasi-lattice constant)	Annealing condition	EPMA composition
P_{40}				
$Al_{72.0}Pd_{16.4}Ru_{11.6}$	*Pa-3*	a = 40.677 (2.822)	1000 ˚C, 48 h	$Al_{72.3}Pd_{15.7}Ru_{12.0}$
P_{20}				
$Al_{70.0}Pd_{22.3}Ru_{7.7}$	*Cubic*	a = 20.269 (2.812)	900 ˚C, 120 h	$Al_{70.3}Pd_{22.3}Ru_{7.4}$
$Al_{70.0}Pd_{22.3}Ru_{6.2}Fe_{1.5}$	*Cubic*	a = 20.231 (2.807)	900 ˚C, 120 h	$Al_{70.9}Pd_{21.7}Ru_{5.7}Fe_{1.6}$
C				
$Al_{72.0}Pd_{16.4}Fe_{11.6}$	*Pm-3*	a = 7.655 (2.781)	900 ˚C, 48 h	$Al_{70.8}Pd_{17.0}Fe_{12.2}$
$Al_{72.0}Pd_{16.4}Ru_{5.8}Fe_{5.8}$	*Pm-3*	a = 7.712 (2.802)	900 ˚C, 48 h	$Al_{71.0}Pd_{15.3}Ru_{8.4}Fe_{5.3}$
ICMs				
$Al_{13}Fe_4$	*C2/m*	a = 15.492 b = 8.078 c = 12.471	1060 ˚C, 120 h	
Al_3Pd_2	*P-3m1*	a = 4.219 c = 5.160	900 ˚C, 120 h	
Al_2Ru	*Fddd*	a = 4.710 b = 7.990 c = 8.760	1000 ˚C, 120 h	

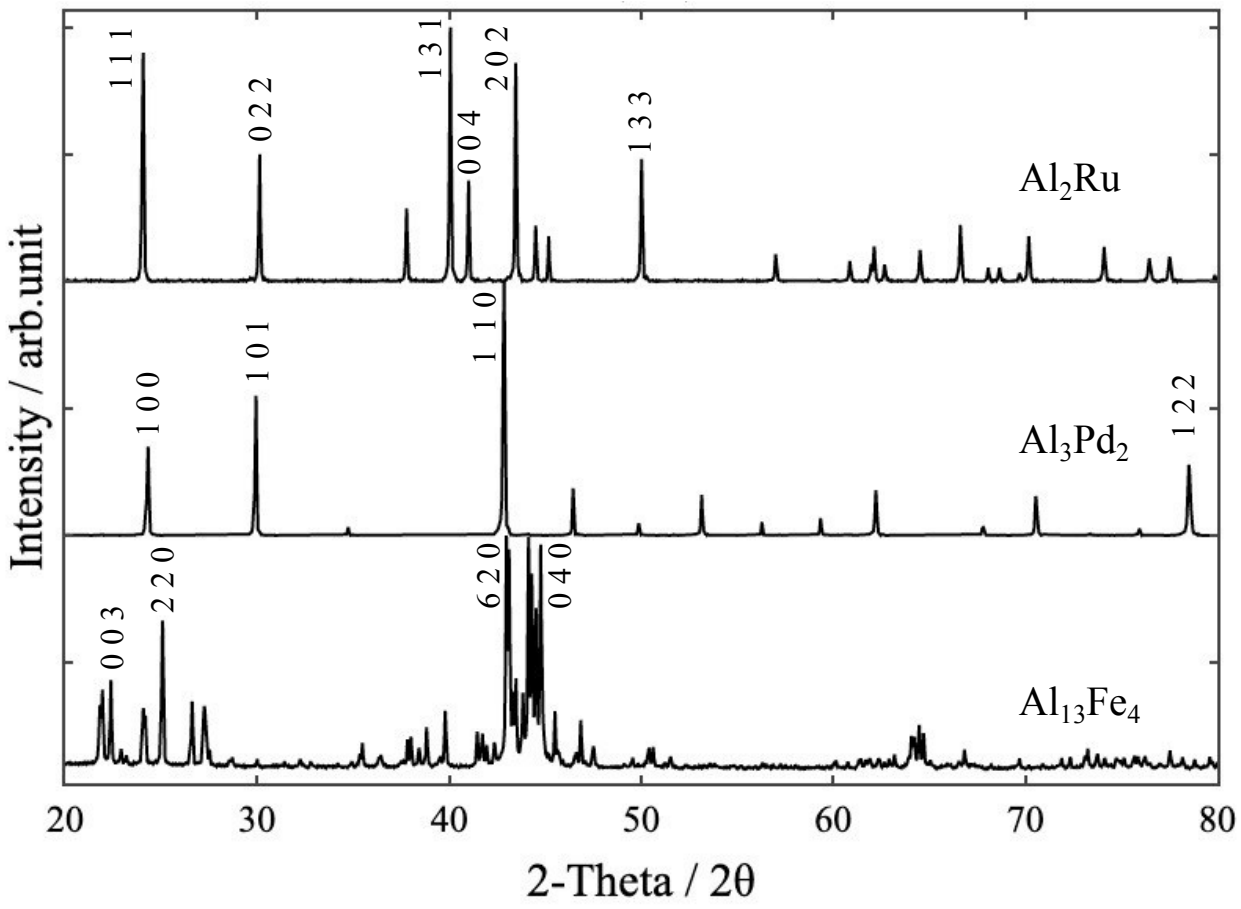

Figure S2. Powder XRD pattern of $Al_{13}Fe_4$, Al_3Pd_2 and Al_2Ru.

2. Characterization.

The phase composition was used the Electron-Probe MicroAnalysis (JEOL JXA-8621MX). The structural analysis was used powder X-ray diffractometer (Rigaku Ultima IV) with Cu-Ka radiation. The confirmation to obtain approximant phase was transmission electron microscopy (TEM) system operated at 200 kV, and sample was powders spread on Cu grids. The specific surface area of powder catalysts was estimated by the Brunauer-Emmett-Teller (BET) method with Kr adsorption after hydrogenation testing. The Al *2s* and Pd *3d* X-ray photoelectron spectra of P_{20}-AlPdRu to confirm surface oxidation were measured at Spring-8 synchrotron, beamline

"BL13XU", with a photon energy of 5949 eV (~6 KeV). The sample was crushed grains with diameter of about 2 mm.

3. Catalytic Test.

The selectivity of C_2H_4 on the C_2H_2 hydrogenation tests was calculated as

$$selectivity = [C_2H_4]_{mol}/([C_2H_4]_{mol} + [C_2H_6]_{mol}) \times 100\%.$$

The conversion of C_2H_2 was translated to reaction rate by using the catalyst surface area (**Table** S2). The reaction rate and selectivity were shown in **Figure S3**. There was included results of all approximants and $Al_{13}Fe_4$ used in this reaction. There was no significant difference in the reaction rates between the approximants with different compositions of P_{40} ($Al_{72.0}Pd_{16.4}Ru_{11.6}$), P_{20} ($Al_{70.0}Pd_{22.3}Ru_{7.7}$), and C ($Al_{72.0}Pd_{16.4}Fe_{11.6}$). Furthermore, no significant difference was caused substitution of Fe to Ru in P_{20} (form $Al_{70.0}Pd_{22.3}Ru_{7.7}$ to $Al_{70.0}Pd_{22.3}Ru_{6.2}Fe_{1.5}$) and that of Ru to Fe in C (from $Al_{72.0}Pd_{16.4}Fe_{11.6}$ to $Al_{72.0}Pd_{16.4}Ru_{5.8}Fe_{5.8}$).

In Fig. 2(a), we have demonstrated our measurements of the reaction rate per unit surface area [mol_{C2H2} s^{-1} m^{-2}-cat] for each sample. Interestingly, we found that the reaction rate of P_{40}-AlPdRu was higher by one order of magnitude than that of $Al_{13}Fe_4$. In fact, the reaction rate would be proportional to turn over frequency (TOF) if the area density of active sites on the surface is assumed to be uniform among measured samples. However, neither dominant crystallographic planes on the exposed surface nor details about the active sites have been clarified. Therefore, it is difficult to estimate the TOF values accurately. At the present stage, we prefer to use the reaction rate per unit surface area [mol_{C2H2} s^{-1} m^{-2}-cat] to TOF.

TOF values over P_{40} and $Al_{13}Fe_4$ were roughly estimated. For example, we found 101 $PdAl_2$ triplet sites within a flat section of a unit cell along a (210) plane, and this gives 0.0565 site/Å^2 as the area density of triplet sites. The number of $PdAl_2$ triplet sites can be estimated to 9.38×10^{-6}

mol_{PdAl2}/m^2-cat (= 0.0565×10^{20} site/m^2-cat. / 6.022×10^{23} site/mol). Turnover frequency (TOF [s^{-1}]) of C_2H_2 hydrogenation based on Fig. 2(a) (5.62×10^{-6} mol_{C2H2}/(s m^2-cat) at 100 °C), which was estimated by assuming that all of $PdAl_2$ triplet sites play as active sites. TOF at 373 K of P40 is *0.599* [s^{-1}] (= 5.62×10^{-6} mol_{C2H2}/(s m^2-cat) / 9.38×10^{-6} mol/m^2-cat). In comparison, TOF at 373 K of $Al_{13}Fe_4$ was estimated to *0.073* [s^{-1}] (= 1.32×10^{-6} mol_{C2H2}/(s m^2-cat) / 1.80×10^{-5} mol/m^2-cat: 1.80×10^{-5} $mol_{triplet}/m^2$-cat).

The selectivity of C_2H_2 on the hydrogenation under industrial like condition was calculated as

$$selectivity = \left([C_2H_{2feed}]_{mol} - [C_2H_2]_{mol}\right)/\left([C_2H_{2feed}]_{mol} - [C_2H_2]_{mol} + [C_2H_6]_{mol}\right) \times 100\%.$$

This C_2H_4 selectivity was calculated that C_2H_2 was assumed to be hydrogenated to C_2H_4 only. In addition, a Lindlar catalyst used for comparison is lead-poisoned palladium 5% on calcium carbonate (TOKYO KASEI KOGYO CO., LTD.). The products and reactants were analyzed by gas chromatography (GC) (Shimadzu, GC-8 A) with a Shincarbon ST column. The conversion was defined as

$$conversion = \left([C_2H_{2feed}]_{mol} - [C_2H_2]_{mol}\right)/[C_2H_{2feed}]_{mol} \times 100\%.$$

Table S2. Sample wight used for catalytic test and surface area after these tests.

Sample	Wight [mg]	Surface area [m^2]
P_{40}		
$Al_{72.0}Pd_{16.4}Ru_{11.6}$	165	0.034(5)
P_{20}		
$Al_{70.0}Pd_{22.3}Ru_{7.7}$	155	0.033(6)
$Al_{70.0}Pd_{22.3}Ru_{6.2}Fe_{1.5}$	144	0.027
C		
$Al_{72.0}Pd_{16.4}Fe_{11.6}$	148	0.041(2)
$Al_{72.0}Pd_{16.4}Ru_{5.8}Fe_{5.8}$	151	0.032
$Al_{13}Fe_4$	151	0.2252

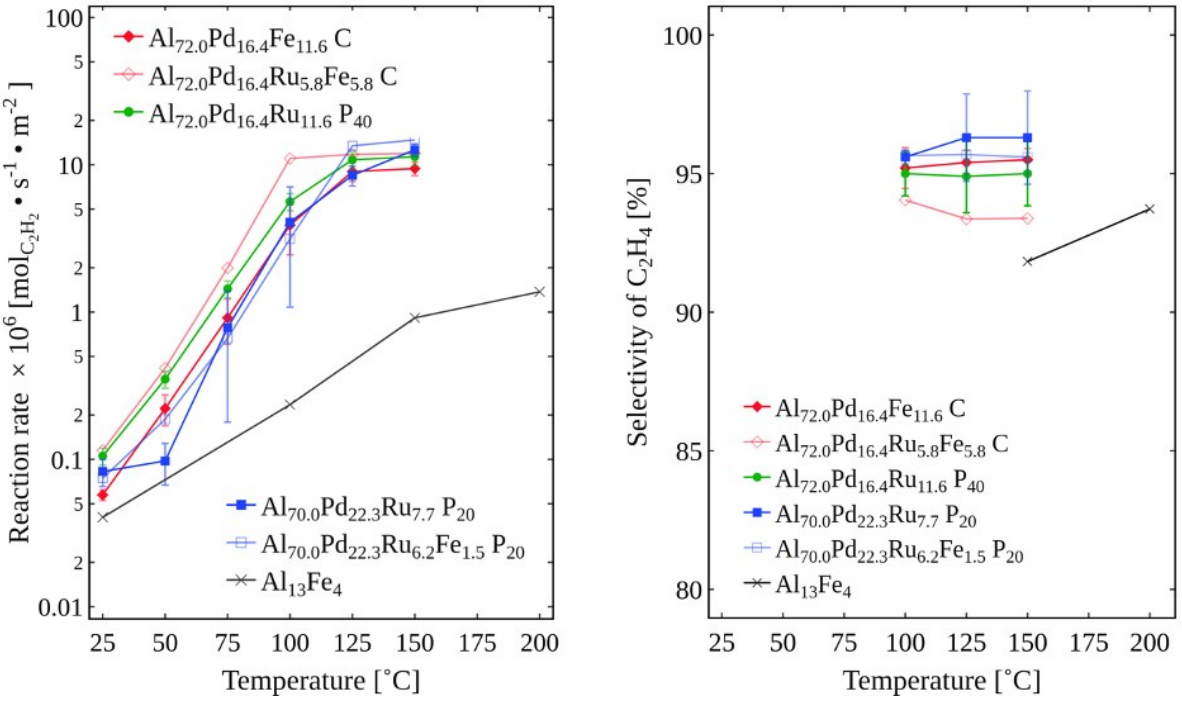

Figure S3. (a) Reaction rate per surface area catalyst and (b) selectivity of C_2H_4 on C_2H_2 hydrogenation tests. The error bar are standard errors obtained from measurement two or three times.

4. Catalytic testing of P_{20} and comparison with simple structure binary IMCs.

A simple structure binary IMCs (Al_3Pd_2, Al_2Ru) and $Al_{70.0}Pd_{22.3}Ru_{7.7}$, P_{20}, were compared to indicate reason that complex approximate crystal structures exhibit high catalytic activity and selectivity. **Figure S4** shows the results of hydrogenation C_2H_2 over Al_3Pd_2, Al_2Ru and P_{20}-AlPdRu (same as Figure 3). The Al_2Ru showed a conversion of less than 10% and a selectivity of about 50%. Al_3Pd_2 with high selectivity comparable to P_{20}-AlPdRu decreased drastically from initial conversion of 85% at 175 ˚C to 30% after 6 h time on stream. Therefore, the high conversion, selectivity and stability are obtained from complex structure of approximants.

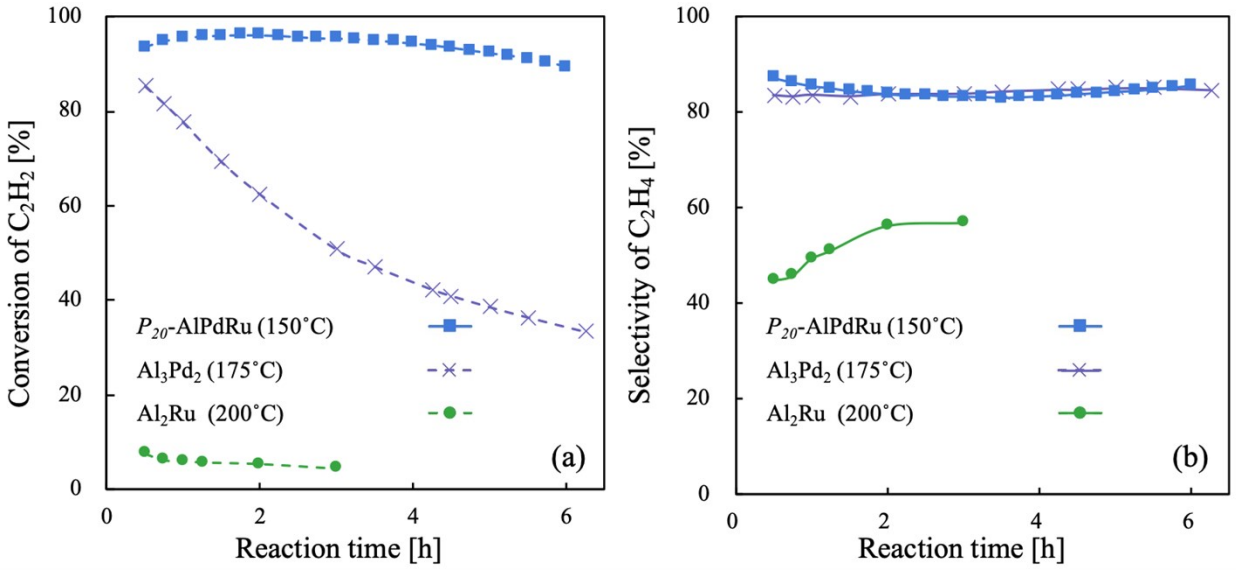

Figure S4. (a) Conversion of C_2H_2 and (b) selectivity of C_2H_4 on Al_3Pd_2, Al_2Ru, and P_{20}-AlPdRu, on stream up to 6 h (reaction gas: 0.5% C_2H_2 / 49% C_2H_4 / 12.5% H_2 in He, total pressure: 0.1 MPa, flow rate: 32 mL/min). Since the activity of Al_2Ru was very low, the test of Al_2Ru was limited to 3 h.

5. Crystal structure of the Al-Pd-TM icosahedral approximants.

The structure of the Al-Pd-TM icosahedral approximants can be understood by placing two kinds of clusters with diameters of ~8 Å at the vertices of a canonical cell tiling (CCT)[S8]. There clusters are called mini-Bergman cluster (mBC) and pseudo-Mackay cluster (pMC), which both have central atom and two polyhedral shells with icosahedral symmetry. The geometrical template of mBC and pMC are shown in **Figure S5 (a)-(d)**. The mBC has been known to consist of inner and outer shells; The inner shell of mBC consists of a regular icosahedron (**Figure S5 (a)**), while the outer shell consists of a regular dodecahedron (**Figure S5 (b)**). The pMC also consists of inner and outer shells. The inner shell of pMC consists of a polyhedral structure with complex site splitting due to very close Al-Al distance (**Figure S5 (c)**). The outer shell of pMC is a composite of a regular icosahedron and a regular icosidodecahedron **(Figure S5 (d)**). The CCT was applied to the structure analysis of Al-Pd-Cr-Fe and P_{40}-Al-Pd-Ru, which was found to have its structure completely filled with mBCs and pMCs (as shown in Figure 3). The structure analysis of *C*-Al-Pd-Fe also showed that all atoms are associated with mBCs and pMCs[S4], as in P_{40}. Although the P_{20} structure is yet unknown, it is expected to be closely related structurally to P_{40} since very similar to the XRD pattern of P_{40} (Figure 1). The high activity and high selectivity of approximants are presumed to attributed to these unique clusters.

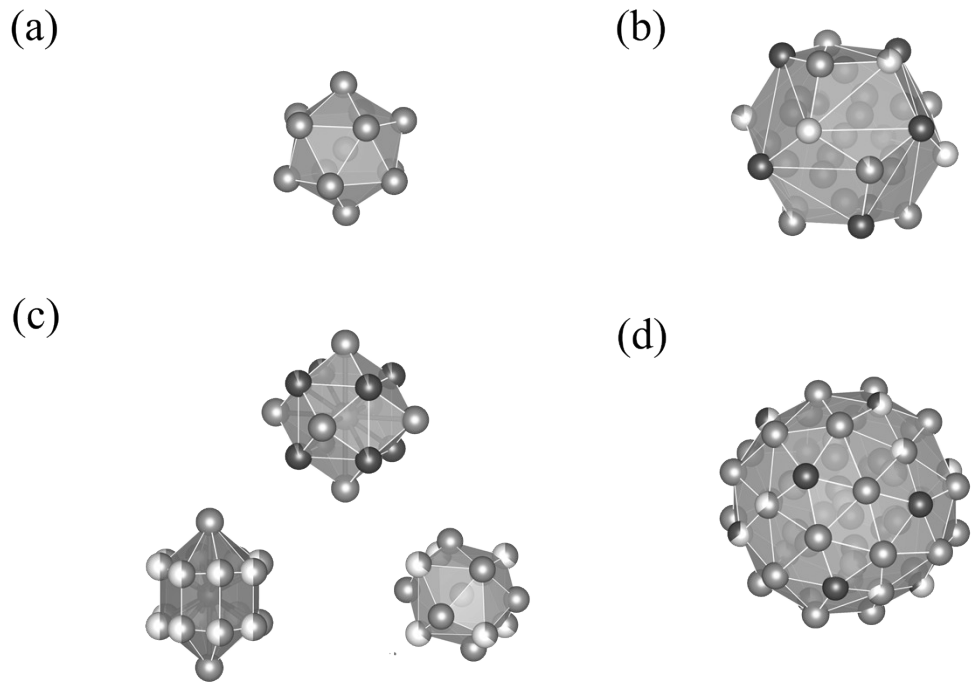

Figure S5 The geomatical template of mBC and pMC. (a) The inner shell of mBC, (b) The outer shell of mBC, (c) The inner shells of pMC, and (d) The outer shell of pMC.

6. Effect of surface oxidation to catalyst.

To control experiment for sample, which was prepared in glove box, P_{20}-AlPdRu, was sieved under air. The catalytic activity of P_{20}-AlPdRu prepared under air was significantly different from that prepared in glove box in **Figure S6**. The samples sieved in air show conversion of 100 % at 100 ˚C to 150 ˚C and remained highly active after 3 h. However, the selectivity of C_2H_4 was dramatically decreased. These results are due to the fact that surface oxidation changed surface structure of the approximants. The XPS spectra of bulk P_{20}-AlPdRu measured under air is show in **Figure S7**. The signals in Al *2s* region of the XPS spectra were assigned to two Al-containing species. There spectra were attributed to pure Al (118 eV) and Al_2O_3 (121 eV), respectively. The signals in Pd *3d* region of the XPS spectra were assigned to only pure Pd as $3d_{5/2}$ (337 eV) and $3d_{3/2}$ (343 eV). It means that the Pd was not affected by oxidation. The surface oxidation by

contacting with air caused surface decomposition of Al_2O_3 and Pd. Therefore, Al_2O_3 and Pd on the oxidation surface resulted the lower selectivity of C_2H_4 in **Figure S6**.

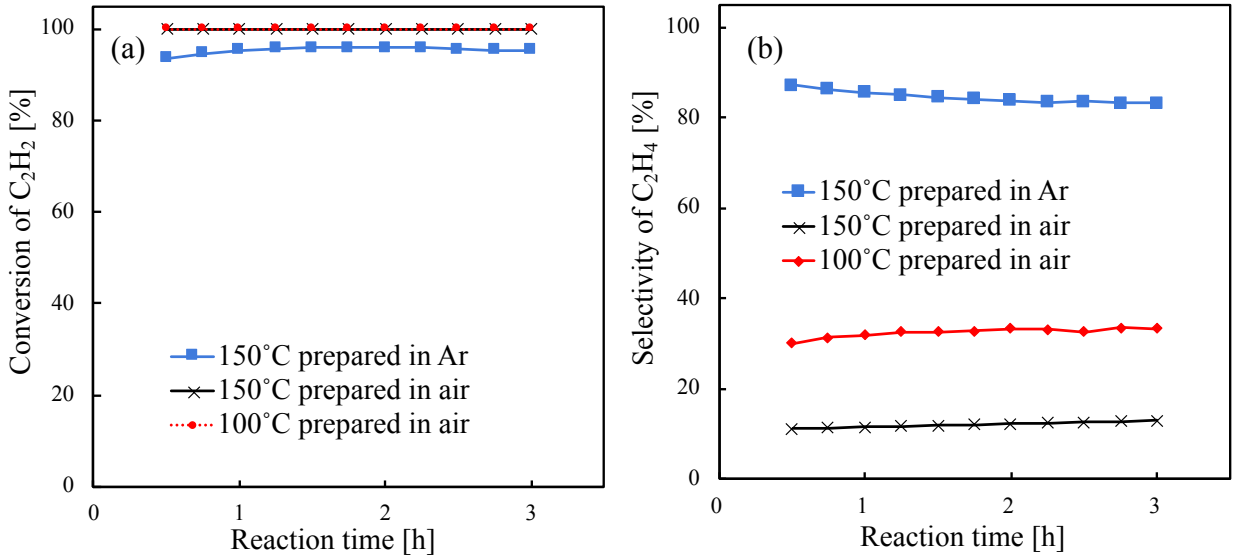

Figure S6. (a) Conversion of C_2H_2 and (b) selectivity of C_2H_4 on P_{20}-AlPdRu phase, Lindlar catalyst and $Al_{13}Fe_4$ (reaction gas: 0.5% C_2H_2/ 49% C_2H_4 / 12.5% H_2 in He, total pressure: 0.1 MPa, flow rate: 32 mL/min).

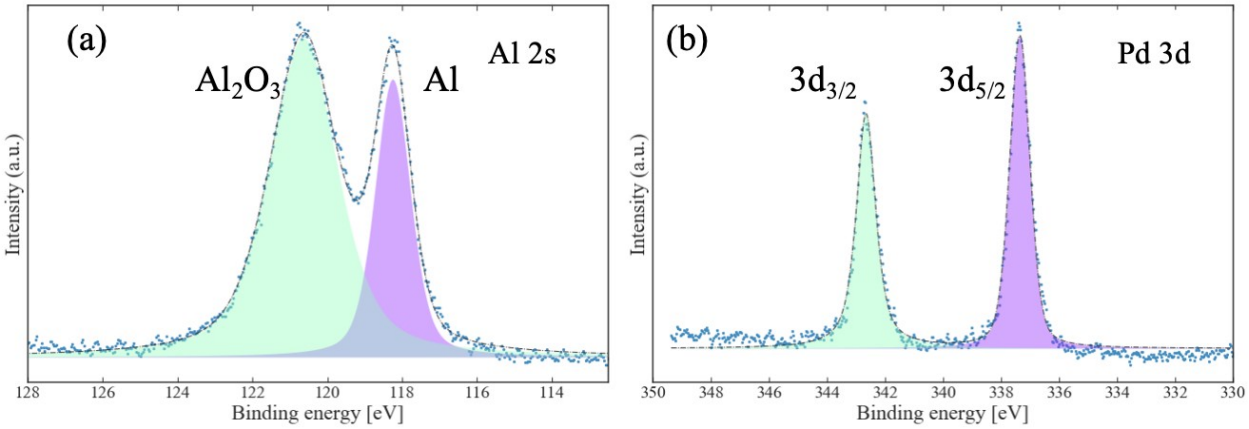

Figure S7. The (a) Al *2s* and (b) Pd *3d* XPS spectra of P_{20}-AlPdRu under air atmosphere

REFERENCES

(S1) Pavlyuchkov, D.; Grushko, B.; Velikanova, T. Ya. An Investigation of the High-Al Part of the Al–Pd–Ru Phase Diagram at 790–900°C. *Journal of Alloys and Compounds* **2009**, *469*, 146–151. DOI:10.1016/j.jallcom.2008.01.138.

(S2) Hatakeyama, Y.; Fujita, N.; Tsai, A. P. Atomic Structure of the Primitive Cubic Phase P_{40} in the Al-Pd-Ru System. *J. Phys.: Conf. Ser.* **2017**, *809*, 012007. DOI:10.1088/1742-6596/809/1/012007.

(S3) Balanetskyy, S.; Grushko, B.; Velikanova, T. Y.; Urban, K. Investigation of the Al–Pd–Fe Phase Diagram between 50 and 100 at.% Al: Ternary Phases. *Journal of Alloys and Compounds* **2004**, *368*, 169–174. DOI:10.1016/j.jallcom.2003.08.034.

(S4) Li, H.; Fan, C. Structure of Cubic $Al_{73.8}Pd_{13.6}Fe_{12.6}$ Phase with High Al Content. *Crystals* **2019**, *9*, 526. DOI:10.3390/cryst9100526.

(S5) Grin, J.; Burkhardt, U.; Ellner, M.; Peters, K. Refinement of the Fe_4Al_{13} Structure and Its Relationship to the Quasihomological Homeotypical Structures. *Z. Kristallogr. Cryst. Mater.* **1994**, *209*, 479–487. DOI:10.1524/zkri.1994.209.6.479.

(S6) Evers, J.; Oehlinger, G.; Meyer, H. Semiconducting Behaviour of $RuGa_2$. *Materials Research Bulletin* **1984**, *19*, 1177–1180. DOI:10.1016/0025-5408(84)90068-0.

(S7) Ellner, M.; Kattner, U.; Predel, B. Konstitutionelle und strukturelle untersuchungen im system Pd-Al. *Journal of the Less Common Metals* **1982**, *87*, 117–133. DOI:10.1016/0022-5088(82)90048-0.

(S8) Fujita, N.; Takano, H.; Yamamoto, A.; Tsai, A.-P. Cluster-Packing Geometry for Al-Based F-Type Icosahedral Alloys. *Acta Crystallogr A Found Crystallogr* **2013**, 69, 322–340. DOI:10.1107/S0108767313005035.

(S9) Krajčí, M.; Hafner, J. Intermetallic Compound AlPd As a Selective Hydrogenation Catalyst: A DFT Study. *J. Phys. Chem. C* **2012**, *116*, 6307–6319. DOI:10.1021/jp212317u.

(S10) Villars, P.; Calvert, L. D. Pearson's Handbook of Crystallographic Data for Intermetallic Phases; American Society for Metals: Metals Park, OH, **1985**.